

Dirac Fermions with Competing Orders: Non-Landau Transition with Emergent Symmetry

Toshihiro Sato, Martin Hohenadler, and Fakher F. Assaad

Institut für Theoretische Physik und Astrophysik, Universität Würzburg, Am Hubland, 97074 Würzburg, Germany

(Dated: October 23, 2017)

We consider a model of Dirac fermions in $2 + 1$ dimensions with dynamically generated, anti-commuting $SO(3)$ Néel and Z_2 Kekulé mass terms that permits sign-free quantum Monte Carlo simulations. The phase diagram is obtained from finite-size scaling and includes a direct and continuous transition between the Néel and Kekulé phases. The fermions remain gapped across the transition, and our data support an emergent $SO(4)$ symmetry unifying the two order parameters. While the bare symmetries of our model do not allow for spinon-carrying Z_3 vortices in the Kekulé mass, the emergent $SO(4)$ invariance permits an interpretation of the transition in terms of deconfined quantum criticality. The phase diagram also features a tricritical point at which Néel, Kekulé, and semimetallic phases meet. The present, sign-free approach can be generalized to a variety of other mass terms and thereby provides a new framework to study exotic critical phenomena.

While some of the seminal theoretical works on symmetry-broken phases of two-dimensional Dirac fermions date back to the 1980s [1, 2], research along these lines was boosted by the experimental realization of graphene [3]. Of particular interest from the perspective of strongly correlated fermions are interaction-driven phase transitions between the semimetal and various ordered phases [4, 5]. The latter include the usual anti-ferromagnet (AFM) [6] and charge-density-wave insulators [1] but also the more complex Kekulé valence-bond solids (KVBSs) [7], as well as quantum Hall and quantum spin Hall states [2, 8, 9]. Remarkably, the Dirac nature of the charge carriers changes the nature of the phase transitions, so that the critical points are described by Gross-Neveu field theories [10] rather than Ginzburg-Landau-Wilson theory [11–18]. Exact quantum Monte Carlo (QMC) simulations have played a key role for our understanding of these phenomena.

The interplay of different order parameters is a fundamental aspect of many-body physics. Whereas phases with different broken symmetries are, in general, connected by intermediate phases or first-order transitions according to Ginzburg-Landau theory, a third possibility exists for quantum phase transitions, namely deconfined quantum critical points (DQCPs). Such DQCPs can be described in terms of emergent spinon degrees of freedom that are confined on either side of the transition but deconfined at criticality [19, 20]. The canonical example is the AFM-VBS critical point of spin- $\frac{1}{2}$ quantum magnets on the square lattice [19, 20] which has been studied numerically using quantum spin or classical loop models [21–23]. Competing orders in Dirac systems have been numerically investigated for spinless ($N = 1$) fermions on the honeycomb lattice [24]. While the topological Mott phase predicted by mean-field theory [9, 25, 26] is destroyed by fluctuations [27], an intricate interplay of different charge- and bond-ordered phases is observed [27–

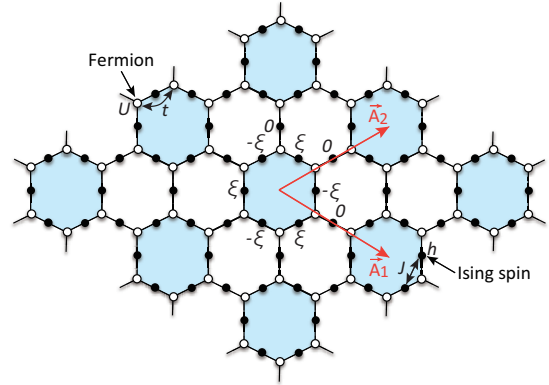


FIG. 1. The model of fermions on the honeycomb lattice with hopping t and Hubbard repulsion U , coupled to Ising spins on the lattice bonds (solid circles) with exchange J and transverse field h . The couplings $\xi_{ij} = 0, \pm\xi$ have a Kekulé modulation. The unit cell (shaded blue) contains six fermionic sites and nine Ising spins. The lattice vectors are \vec{A}_1 and \vec{A}_2 .

31]. For $N = 2$, the semimetal-AFM transition [6, 16–18, 32, 33] and the semimetal-KVBS transition [34] were investigated by QMC simulations (for the case $N > 2$ see Refs. [35, 36]). However, no QMC results exist for competing order parameters because a sign problem arises in simulations of minimal extended Hubbard models.

In this Letter, we apply exact QMC simulations to a model of $N = 2$ Dirac fermions in $2 + 1$ dimensions that captures the interplay of the chiral $SO(3)$ Néel mass term and an Ising-type Kekulé mass term. We present the phase diagram and evidence for a direct, second-order quantum phase transition between the two ordered states with an emergent $SO(4)$ symmetry at criticality related to the anticommuting nature of the mass terms.

Model.—To study the competition between the Néel and Kekulé mass terms, we simulated a honeycomb lat-

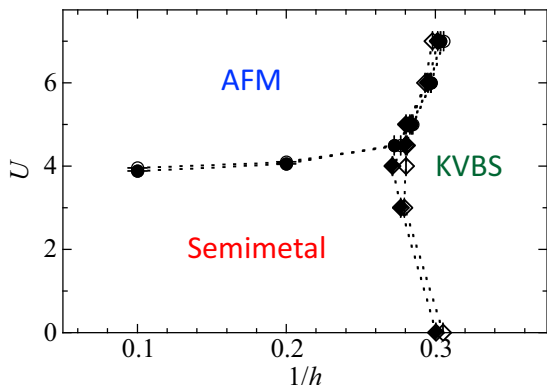


FIG. 2. Phase diagram with semimetallic, antiferromagnetic (AFM) and Kekulé-ordered (KVBS) phases from QMC simulations at $T = 0.05$. Circles (diamonds) indicate the onset of long-range Néel (Kekulé) order; open (solid) symbols are critical values based on $L = 3$ and 6 ($L = 6$ and 9), see text.

tice model with Hamiltonian $\hat{H} = \hat{H}_f + \hat{H}_s + \hat{H}_{fs}$. Here,

$$\hat{H}_f = -t \sum_{\langle ij \rangle, \sigma} \hat{c}_{i\sigma}^\dagger \hat{c}_{j\sigma} + U \sum_i (\hat{n}_{i\uparrow} - \frac{1}{2})(\hat{n}_{i\downarrow} - \frac{1}{2}) \quad (1)$$

corresponds to the Hubbard model, whereas

$$\hat{H}_s = J \sum_{\langle ij, kl \rangle} \hat{s}_{ij}^z \hat{s}_{kl}^z - h \sum_{\langle ij \rangle} \hat{s}_{ij}^x \quad (2)$$

is a ferromagnetic, transverse-field Ising model defined on the bonds $\langle ij \rangle$ of the honeycomb lattice. The fermion-spin coupling ($\xi_{ij} = 0, \pm\xi$, see Fig. 1) is given by

$$\hat{H}_{fs} = \sum_{\langle ij \rangle, \sigma} \xi_{ij} \hat{s}_{ij}^z \hat{c}_{i\sigma}^\dagger \hat{c}_{j\sigma}. \quad (3)$$

It defines a new unit cell with lattice vectors \vec{A}_1 and \vec{A}_2 and allows for scattering between the Dirac cones and thereby Kekulé order. The full model has an $SU(2)$ spin symmetry as well as a Z_2 symmetry corresponding to invariance under the combined operation of inversion and $\hat{s}_{ij}^z \rightarrow -\hat{s}_{ij}^z$. Since $\hat{H}_{fs} \rightarrow -\hat{H}_{fs}$ under inversion (or reflection across the y axis), the energy does not depend on the sign of ξ and the two possible Kekulé patterns related by $\xi \rightarrow -\xi$ are degenerate.

The Hubbard interaction and the spin-fermion coupling (3) have the potential to generate Néel and Kekulé order, respectively. Within the framework of Ginzburg-Landau theory, and in the notation of Ref. [12], a minimal low-energy theory of Dirac fermions with Néel and Kekulé mass terms is given by the Lagrangian

$$\mathcal{L} = \sum_{\sigma\sigma'} \bar{\Psi}_\sigma \left[\partial_u \gamma_u \delta_{\sigma\sigma'} + \begin{pmatrix} \mathbf{m}_{\text{AFM}} \\ m_{\text{KVBS}} \end{pmatrix} \cdot \begin{pmatrix} \boldsymbol{\sigma}_{\sigma\sigma'} \\ i\gamma_5 \delta_{\sigma\sigma'} \end{pmatrix} \right] \Psi_{\sigma'}, \quad (4)$$

plus a purely bosonic part \mathcal{L}_b that captures fluctuations of the individual masses as well as the coupling between

them. Note that the second possible Kekulé mass term on the honeycomb lattice, $i\gamma_0\gamma_3$ [7], is forbidden in our construction since it is even under inversion.

Our Hamiltonian \hat{H} captures the physics of competing, dynamically generated order parameters described by Eq. (4). The introduction of Ising spins is simply a means of defining a model with the desired low-energy theory, while at the same time avoiding the minus-sign problem and hence opening the way to large-scale QMC simulations; the absence of a sign problem is due to particle-hole symmetry [37]. This designer Hamiltonian approach is extremely flexible. For instance, similar sign-free models have recently been introduced to study, e.g., nematic [38] and ferromagnetic transitions in metals [39], topological Mott insulators [40], and Z_2 lattice gauge theories coupled to matter [41, 42].

Method.—We used the ALF (Algorithms for Lattice Fermions) implementation [43] of the well-established finite-temperature auxiliary-field QMC method [44, 45]. A temperature $T = 0.05$ (with Trotter discretization $\Delta\tau = 0.1$) was sufficient to obtain results representative of the ground state. We simulated half-filled lattices with $L \times L$ unit cells ($V = 6L^2$ sites) and periodic boundary conditions. Henceforth, we use $t = 1$ as the energy unit, set $J = -1$ and $\xi = 0.5$.

Phase diagram.—The phase diagram shown in Fig. 2 was obtained from a finite-size scaling analysis. We measured equal-time correlation functions of fermion spin operators $\hat{S}_i = \sum_{\sigma\sigma'} \hat{c}_{i\sigma}^\dagger \boldsymbol{\sigma}_{\sigma\sigma'} \hat{c}_{i\sigma}$, fermion bond operators $\hat{B}_{ij} = -t \sum_{\sigma} (\hat{c}_{i\sigma}^\dagger \hat{c}_{j\sigma} + \hat{c}_{j\sigma}^\dagger \hat{c}_{i\sigma})$, and Ising spin operators \hat{s}_{ij}^z . Because of the larger unit cell, these correlators are matrices of the form $C_{i\gamma, j\delta}^O$ with site indices i, j and bond indices γ, δ . After diagonalizing the corresponding structure factors $C_{\gamma\delta}^O(\mathbf{q}) = \frac{1}{V} \sum_{ij} C_{i\gamma, j\delta}^O e^{i\mathbf{q} \cdot (\mathbf{R}_i - \mathbf{R}_j)}$, we calculated the correlation ratios ($O = \mathbf{S}, B, s$) [46, 47]

$$R_O = 1 - \frac{\lambda_1(\mathbf{q}_0 + \delta\mathbf{q})}{\lambda_1(\mathbf{q}_0)} \quad (5)$$

using the largest eigenvalue $\lambda_1(\mathbf{q})$; \mathbf{q}_0 is the ordering wave vector, $\mathbf{q}_0 + \delta\mathbf{q}$ a neighboring wave vector. By definition, $R_O \rightarrow 1$ for $L \rightarrow \infty$ in the corresponding ordered phase, whereas $R_O \rightarrow 0$ in the disordered phase. At the critical point, R_O is scale invariant for sufficiently large L and results for different system sizes cross [46, 47].

Figure 3 shows results at $U = 6$. The onset of long-range Néel order is detected from the crossing of $R_{\text{AFM}} \equiv R_{\mathbf{S}}$ [Fig. 3(a)]. The onset of Kekulé order can be detected either from $R_{\text{KVBS}} \equiv R_s$ [shown in Fig. 3(b)] or from R_B . The crossings yield a consistent estimate of the critical point of $1/h_c \approx 0.29$. The same analysis was carried out for other parameters to construct the phase diagram. The phase boundaries in Fig. 2 are based on the crossing points of results for $L = 3, 6$ (open symbols) and $L = 6, 9$ (solid symbols), respectively.

Because the semimetal is stable with respect to weak perturbations [11], phase transitions occur at nonzero

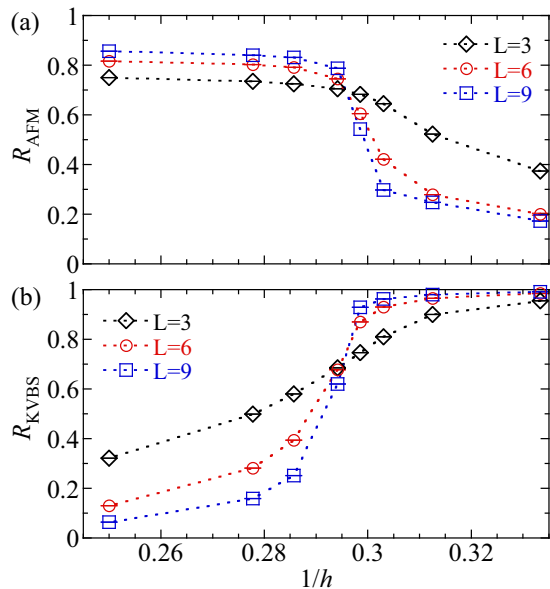


FIG. 3. Correlation ratios for (a) antiferromagnetic order and (b) Kekulé order across the AFM-KVBS transition at $U = 6$. The crossings yield a critical value of $1/h_c \approx 0.29$.

couplings. Accordingly, the phase diagram in Fig. 2 shows an extended semimetallic phase as well as ordered AFM and KVBS phases. Whereas the semimetal preserves the relevant $SO(3) \times Z_2$ symmetry of our model, the AFM breaks the $SO(3)$ spin symmetry and the KVBS with long-range Kekulé order (and ferromagnetic order of the Ising spins) breaks the Z_2 symmetry. The most interesting aspect of Fig. 2 is the direct transition between the AFM and the KVBS, with a potential tricritical point at $(U, 1/h) \approx (4.2, 0.28)$. The slight mismatch of critical values near this point is within the finite-size uncertainties and does not imply an intermediate phase. Further evidence for a direct transition will be presented below. The semimetal-AFM and semimetal-KVBS transitions are expected to be in the previously studied Gross-Neveu-Heisenberg [14, 17, 18] and Gross-Neveu-Ising [40] universality classes, respectively. Their critical values are only slightly changed by the fermion-spin coupling. The AFM-KVBS transition at $U = 6$ will be the focus of the remainder of this Letter.

AFM-KVBS transition.—The results of Fig. 3 suggest a single critical point, with the scaling behavior pointing to a continuous transition. Additional evidence can be obtained from the free-energy derivative $\partial F/\partial h = \langle \sum_{\langle ij \rangle} s_{ij}^x \rangle$ in Fig. 4(a), reveals no signs of discontinuous behavior for the system sizes accessible. Similar results were found at lower temperatures. We also analyzed the single-particle gap across the transition and found it to remain clearly nonzero [Fig. 4(b)].

The fact that the two mass terms considered anticommute has important consequences. They can be combined [see Eq. (4)] into a four-component order param-

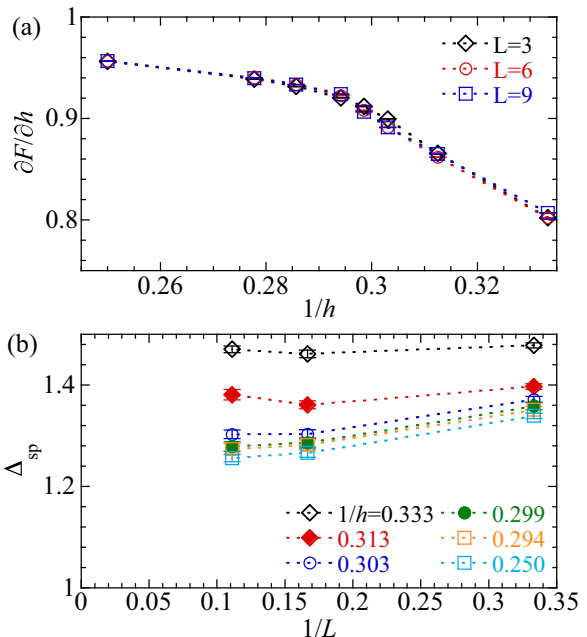


FIG. 4. (a) Free-energy derivative $\partial F/\partial h$ and (b) single-particle gap Δ_{sp} at the Dirac point. Here, $U = 6$.

eter $\mathbf{m} = (m_{\text{AFM}}, m_{\text{KVBS}})$ in terms of which the Hartree-Fock gap at the Dirac points is $\Delta_{sp} = |\mathbf{m}|$. In the AFM the vector \mathbf{m} lies in the \mathbb{R}^3 subspace spanned by its first three components, whereas in the KVBS it is pinned along the fourth direction. Our observation of a continuous transition at which $|\mathbf{m}|$ (and hence Δ_{sp}) does not vanish implies that \mathbf{m} becomes unpinned at the transition and averages to zero. Within this picture, the four components of the vector \mathbf{m} are related by a chiral rotation at criticality and the system should exhibit an emergent $SO(4)$ symmetry. While, in principle, the second $i\gamma_0\gamma_3$ Kekulé mass could be generated dynamically, we verified that the transition involves only the $i\gamma_0\gamma_5$ mass. We therefore expect an $SO(4)$ rather than an $SO(5)$ symmetry.

The full low-energy theory includes the $SO(4)$ symmetric terms of Eq. (4) as well as contributions that break this symmetry. To verify whether the critical point has an emergent $SO(4)$ symmetry we follow Ref. [23] and consider the standard deviations $\sigma_O = \sqrt{\langle O^2 \rangle - \langle O \rangle^2}$ of the AFM ($\sigma_{\text{AFM}} \equiv \sigma_S$) and KVBS ($\sigma_{\text{KVBS}} \equiv \sigma_s$) order parameters. While these quantities are, in general, independent, they become locked together if an $SO(4)$ symmetry emerges. Therefore, the ratio $\sigma_{\text{KVBS}}/\sigma_{\text{AFM}}$ should become universal at the critical point $1/h_c \approx 0.29$, which is exactly what we see in Fig. 5. The emergent symmetry can also be observed in the joint probability distribution of the two order parameters. Given $SO(4)$ symmetry, the latter depends only on $|\mathbf{m}_{\text{AFM}}|^2 + m_{\text{KVBS}}^2 = |\mathbf{m}|^2$. Accordingly, a histogram determined from QMC snapshots should (after normalization) produce a circular distribu-

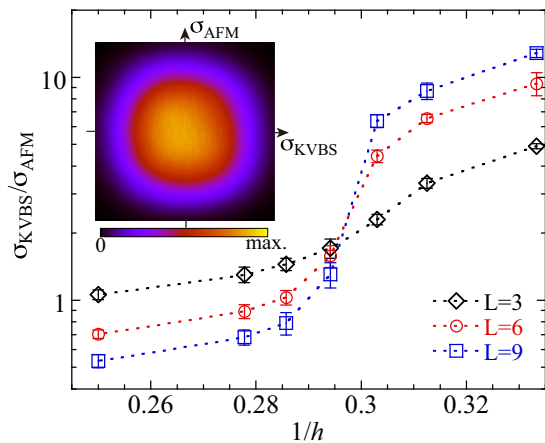


FIG. 5. Ratio of the standard deviations of the AFM and KVBS order parameters. Inset: Joint (normalized) probability distribution of the two order parameters near the critical point ($1/h_c = 0.29$) for $L = 6$. Here, $U = 6$.

tion [21, 23]. This is confirmed by the inset in Fig. 5. These results also provide further evidence for the continuous nature of the AFM-KVBS transition.

Discussion.—We have shown numerically that Dirac fermions with competing Néel and Kekulé order parameters can exhibit a Landau-forbidden, direct and continuous transition with emergent $SO(4)$ symmetry. The key ingredient underlying this behavior is the anticommutativity of the two mass terms.

We first discuss the relation of our findings to DQCPs [20] described by noncompact- CP^1 (NCCP¹) field theory for spinons deconfined at criticality. For the KVBS on the honeycomb lattice, the spinons can be identified with isolated spin- $\frac{1}{2}$ degrees of freedom at the center of Z_3 vortices in the Kekulé order parameter [48]. This intuitive picture was first proposed by Levin and Senthil [49] for the C_4 symmetric case. Interestingly, there is numerical evidence that models without low-energy spinons carried by Z_3 vortices exhibit strongly first-order AFM-KVBS transitions [50, 51]. Our choice of model only allows one of the two Kekulé mass terms, thereby excluding the possibility of spinon-carrying Z_3 vortices and suggesting a first-order AFM-KVBS transition.

The emergent $SO(4)$ symmetry allows us to understand the observed, continuous AFM-KVBS transition in terms of a DQCP. Because the single-particle gap remains open across the transition, the fermions can be integrated out to obtain a purely bosonic theory with topological terms [52, 53]. In the present case, this yields a four-component nonlinear sigma model with a θ -term at $\theta = \pi$ that describes the winding of the normalized 4D mass vector \mathbf{m} on the 3D space-time sphere. This bosonic theory has been argued to be equivalent to the NCCP¹ field theory [54]. Very recent numerical simulations [55] aimed at confirming duality relations [56] reveal that the quantum phase transition between an XY AFM and a VBS is

continuous and has an emergent $SO(4)$ symmetry. This result was obtained using the easy-axis J - Q model which has a bare $U(1) \times C_4$ symmetry [55], compared to the $SO(3) \times Z_2$ symmetry of our model. Because both models are described by the same effective field theory at criticality, the AFM-(K)VBS transitions should be in the same universality class, in accordance with a preliminary finite-size scaling analysis. The emergent symmetry observed in numerical results for the AFM-VBS DQCP in models that support spinons may be regarded as an interesting but secondary feature that does not enter in the field-theory description. By contrast, our findings suggest that it plays a central role in realizing a DQCP in models whose bare symmetries do not support spinon excitations.

Outlook.—We used a fermionic QMC method that scales with the cube of the volume and hence is limited regarding the accessible system sizes. Because the AFM-KVBS transition is described by a bosonic theory, it seems possible to instead start with Dirac fermions with anticommuting mass terms and derive spin models that do not support spinon-carrying Z_3 vortices. Such models can be simulated on large lattices without a sign problem in the stochastic series expansion representation [57] to verify our conclusions. Another fruitful direction for future work is a detailed understanding of critical behavior at and away from the tricritical point [58]. Finally, the model considered here is only one of many possible sign-free Hamiltonians that can be simulated to investigate Dirac fermions with multiple mass terms.

We thank T. Grover, I. Herbut, L. Janssen, C. Mudry, N. Prokof'ev, B. Roy, S. Sachdev, M. Scherer and T. Senthil for helpful discussions. This work was supported by the Deutsche Forschungsgemeinschaft through SFB 1170 ToCoTronics and FOR 1807. We gratefully acknowledge the Gauss Centre for Supercomputing (GCS) for allocation of CPU time on the SuperMUC computer at the Leibniz Supercomputing Center as well as the John von Neumann Institute for Computing (NIC) for computer resources on the JURECA [59] machine at the Jülich Supercomputing Centre (JSC).

-
- [1] G. W. Semenoff, Phys. Rev. Lett. **53**, 2449 (1984).
 - [2] F. D. M. Haldane, Phys. Rev. Lett. **61**, 2015 (1988).
 - [3] K. S. Novoselov, A. K. Geim, S. V. Morozov, D. Jiang, M. I. Katsnelson, I. V. Grigorieva, S. V. Dubonos, and A. A. Firsov, Nature **438**, 197 (2005).
 - [4] I. F. Herbut, Phys. Rev. Lett. **97**, 146401 (2006).
 - [5] S. Ryu, C. Mudry, C.-Y. Hou, and C. Chamon, Phys. Rev. B **80**, 205319 (2009).
 - [6] S. Sorella and E. Tosatti, Europhys. Lett. **19**, 699 (1992).
 - [7] C.-Y. Hou, C. Chamon, and C. Mudry, Phys. Rev. Lett. **98**, 186809 (2007).
 - [8] C. L. Kane and E. J. Mele, Phys. Rev. Lett. **95**, 146802 (2005).

- [9] S. Raghu, X.-L. Qi, C. Honerkamp, and S.-C. Zhang, *Phys. Rev. Lett.* **100**, 156401 (2008).
- [10] D. J. Gross and A. Neveu, *Phys. Rev. D* **10**, 3235 (1974).
- [11] I. F. Herbut, V. Juričić, and B. Roy, *Phys. Rev. B* **79**, 085116 (2009).
- [12] I. F. Herbut, V. Juričić, and O. Vafek, *Phys. Rev. B* **80**, 075432 (2009).
- [13] P. Ghaemi and S. Ryu, *Phys. Rev. B* **85**, 075111 (2012).
- [14] F. F. Assaad and I. F. Herbut, *Phys. Rev. X* **3**, 031010 (2013).
- [15] L. Wang, P. Corboz, and M. Troyer, *New J. Phys.* **16**, 103008 (2014).
- [16] M. Hohenadler, F. Parisen Toldin, I. F. Herbut, and F. F. Assaad, *Phys. Rev. B* **90**, 085146 (2014).
- [17] F. Parisen Toldin, M. Hohenadler, F. F. Assaad, and I. F. Herbut, *Phys. Rev. B* **91**, 165108 (2015).
- [18] Y. Otsuka, S. Yunoki, and S. Sorella, *Phys. Rev. X* **6**, 011029 (2016).
- [19] T. Senthil, L. Balents, S. Sachdev, A. Vishwanath, and M. P. A. Fisher, *Phys. Rev. B* **70**, 144407 (2004).
- [20] T. Senthil, A. Vishwanath, L. Balents, S. Sachdev, and M. P. Fisher, *Science* **303**, 1490 (2004).
- [21] A. W. Sandvik, *Phys. Rev. Lett.* **98**, 227202 (2007).
- [22] L. Wang, Z.-C. Gu, F. Verstraete, and X.-G. Wen, *Phys. Rev. B* **94**, 075143 (2016).
- [23] A. Nahum, P. Serna, J. T. Chalker, M. Ortuño, and A. M. Somoza, *Phys. Rev. Lett.* **115**, 267203 (2015).
- [24] S. Capponi, *J. Phys.: Condens. Matter* **29**, 043002 (2017).
- [25] C. Weeks and M. Franz, *Phys. Rev. B* **81**, 085105 (2010).
- [26] A. G. Grushin, E. V. Castro, A. A Cortijo, F. de Juan, M. A. H. Vozmediano, and B. Valenzuela, *Phys. Rev. B* **87**, 085136 (2013).
- [27] M. Daghofer and M. Hohenadler, *Phys. Rev. B* **89**, 035103 (2014).
- [28] N. A. García-Martínez, A. G. Grushin, T. Neupert, B. Valenzuela, and E. V. Castro, *Phys. Rev. B* **88**, 245123 (2013).
- [29] T. Durić, N. Chancellor, and I. F. Herbut, *Phys. Rev. B* **89**, 165123 (2014).
- [30] S. Capponi and A. M. Läuchli, *Phys. Rev. B* **92**, 085146 (2015).
- [31] J. Motruk, A. G. Grushin, F. de Juan, and F. Pollmann, *Phys. Rev. B* **92**, 085147 (2015).
- [32] Z. Y. Meng, T. C. Lang, S. Wessel, F. F. Assaad, and A. Muramatsu, *Nature* **464**, 847 (2010).
- [33] S. Sorella, Y. Otsuka, and S. Yunoki, *Sci. Rep.* **2**, 992 (2012).
- [34] Z.-X. Li, Y.-F. Jiang, S.-K. Jian, and H. Yao, *Nat. Commun.* **8**, 314 (2017).
- [35] T. C. Lang, Z. Y. Meng, A. Muramatsu, S. Wessel, and F. F. Assaad, *Phys. Rev. Lett.* **111**, 066401 (2013).
- [36] Z. Zhou, D. Wang, Z. Y. Meng, Y. Wang, and C. Wu, *Phys. Rev. B* **93**, 245157 (2016).
- [37] C. Wu and S.-C. Zhang, *Phys. Rev. B* **71**, 155115 (2005).
- [38] Y. Schattner, S. Lederer, S. A. Kivelson, and E. Berg, *Phys. Rev. X* **6**, 031028 (2016).
- [39] X. Y. Xu, K. Sun, Y. Schattner, E. Berg, and Z. Y. Meng, *Phys. Rev. X* **7**, 031058 (2017).
- [40] Y.-Y. He, X. Y. Xu, K. Sun, F. F. Assaad, Z. Y. Meng, and Z.-Y. Lu, arXiv:1705.09192 (2017).
- [41] F. F. Assaad and T. Grover, *Phys. Rev. X* **6**, 041049 (2016).
- [42] S. Gazit, M. Randeria, and A. Vishwanath, *Nature Phys.* **13**, 484 (2017).
- [43] M. Bercx, F. Goth, J. S. Hofmann, and F. F. Assaad, *SciPost* **3**, 013 (2017).
- [44] R. Blankenbecler, D. J. Scalapino, and R. L. Sugar, *Phys. Rev. D* **24**, 2278 (1981).
- [45] F. F. Assaad and H. G. Evertz, in *Computational Many Particle Physics, Lecture Notes in Physics*, Vol. 739, edited by H. Fehske, R. Schneider, and A. Weiße (Springer Verlag, 2008) p. 277.
- [46] K. Binder, *Z. Phys. B Con. Mat.* **43**, 119 (1981).
- [47] S. Pujari, T. C. Lang, G. Murthy, and R. K. Kaul, *Phys. Rev. Lett.* **117**, 086404 (2016).
- [48] S. Pujari, K. Damle, and F. Alet, *Phys. Rev. Lett.* **111**, 087203 (2013).
- [49] M. Levin and T. Senthil, *Phys. Rev. B* **70**, 220403 (2004).
- [50] A. Sen and A. W. Sandvik, *Phys. Rev. B* **82**, 174428 (2010).
- [51] A. Banerjee, K. Damle, and A. Paramekanti, *Phys. Rev. B* **83**, 134419 (2011).
- [52] A. Abanov and P. Wiegmann, *Nucl. Phys. B* **570**, 685 (2000).
- [53] A. Tanaka and X. Hu, *Phys. Rev. Lett.* **95**, 036402 (2005).
- [54] T. Senthil and M. P. A. Fisher, *Phys. Rev. B* **74**, 064405 (2006).
- [55] Y. Q. Qin, Y.-Y. He, Y.-Z. You, Z.-Y. Lu, A. Sen, A. W. Sandvik, C. Xu, and Z. Y. Meng, *Phys. Rev. X* **7**, 031052 (2017).
- [56] C. Wang, A. Nahum, M. A. Metlitski, C. Xu, and T. Senthil, *Phys. Rev. X* **7**, 031051 (2017).
- [57] A. W. Sandvik, *Phys. Rev. Lett.* **104**, 177201 (2010).
- [58] B. Roy, *Phys. Rev. B* **84**, 113404 (2011).
- [59] Jülich Supercomputing Centre (2016), in *JURECA: General-purpose supercomputer at Jülich Supercomputing Centre, Journal of Large-Scale Research Facilities*, Vol. 2, p. A62, <http://dx.doi.org/10.17815/jlsrf-2-121>.